THE JOURNAL OF PHYSICAL CHEMISTRY C

Article

pubs.acs.org/JPCC

Bidirectional Ion Emission from Massive Gold Cluster Impacts on Nanometric Carbon Foils

J. Daniel DeBord,[†] Serge Della-Negra,[‡] Francisco A. Fernandez-Lima,[†] Stanislav V. Verkhoturov,[†] and Emile A. Schweikert*,[†]

[†]Department of Chemistry, Texas A&M University, College Station, Texas 77943-3144, United States

[‡]Institut de Physique Nucléaire d'Orsay, Université Paris-Sud 11, CNRS/IN2P3, F-91406 Orsay, France

ABSTRACT: Carbon cluster emission from thin carbon foils (5−40 nm) impacted by individual Au_n^{+q} cluster projectiles (95−125 qkeV, n/q = 3−200) reveals features regarding the energy deposition, projectile range, and projectile fate in the matter as a function of the projectile characteristics. For the first time, the secondary ion emission from thin foils has been monitored simultaneously in both forward and backward emission directions. The projectile range and depth of emission were examined as a function of projectile size, energy, and target thickness. A key finding is that the massive cluster impact develops very differently from that of a small polyatomic projectile. The range of the 125 qkeV Au_{100q}^{+q} ($q \approx 4$) projectile is estimated to be 20 nm (well beyond the range of an equal velocity Au^+), and projectile disintegration occurs at the exit of even a 5 nm thick foil.

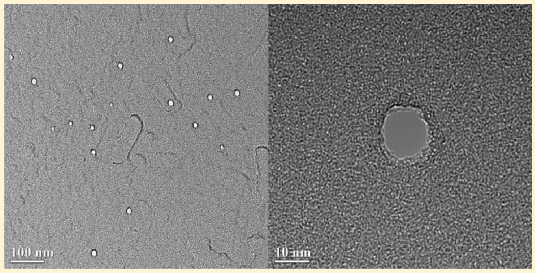

1. INTRODUCTION

It has long been recognized that the impact of hypervelocity massive clusters on solids differs in the resultant dynamics from those occurring for atomic or small cluster ions of comparable velocities.[1−4] Yet, little is known about this impact regime, beyond observations of impact craters/holes and reports of abundant secondary ion (SI) emission.[5−7] Visualization of impacts of individual massive clusters, e.g., 100 water molecule ions or Au_n^{+q} ($100 \le n \le 1000$; q = 1−10) at velocities of 10 to 100 km/s on thin carbon films shows craters of size and depth roughly correlated with the projectile size and energy.[8−10] Remarkably, their range significantly exceeds that of equal velocity atomic ions, a feature attributed to the clearing-the-way effect.[11,12] This effect is not observed for polyatomic ions with up to seven atoms[13] but is observed in simulations of 13 atoms.[14] The effect also seems to disappear for projectiles with >200 keV/atom.[15] The morphological observations and molecular dynamic simulations indicate an energy deposition process in a hydrodynamic flow.[16] A distinct characteristic of the massive cluster solid impact is the extreme energy density and pressure transient. This provides a medium for chemical reactions under nonclassical conditions as they may occur, for example, in impacts of hypervelocity nanosized dust particles in interstellar space.[17]

Data from previous impact experiments and simulations are unidirectional, that is, they either record the surface morphology or ejecta from the impact side, or they document projectile transmission with visualization of holes in carbon foils or excisions in virus particles.[18] In this study, we recorded the concurrent SI emission in both directions from a thin carbon foil so that we could evaluate the parameters of the massive cluster−solid interaction, which affect the SI emission, with particular attention given to the projectile size and target thickness.

2. EXPERIMENTAL SECTION

2.1. Instrumental Setup. A schematic for the experimental setup is shown in Figure 1. The instrument consists of a dual time-of-flight (ToF) mass spectrometer, which permits the analysis of SIs emitted from both sides of a thin carbon foil bombarded by massive clusters. A negative accelerating potential is applied to the thin foil sample, while 90% transmission grids on either side of the target are maintained at the ground. The transmission and detection efficiencies are equivalent for both ToF legs. For the presentation and discussion of the results, we have decided to designate SI ejection back in the direction of incoming projectiles as backward emission and SI ejection in the opposite direction where, for some experiments, the projectiles exit the foil as forward emission. The impact of a massive cluster is detected via electron emission in the backward direction after magnetic deflection. The electron signal given by a microchannel plate detector serves as the start for both the forward and backward ToF measurements. This procedure creates the same impact trigger independent of sample thickness and avoids artifacts from holes in the foils. In order to monitor the fate of projectiles that pass through the foil, a second thin foil is utilized. For these experiments, both foils are positioned between the grounded extraction grids with the distance between the two foils estimated at 100 μm.

Received: December 15, 2011
Revised: March 7, 2012
Published: March 12, 2012

   dx.doi.org/10.1021/jp212126m | J. Phys. Chem. C 2012, 116, 8138−8144

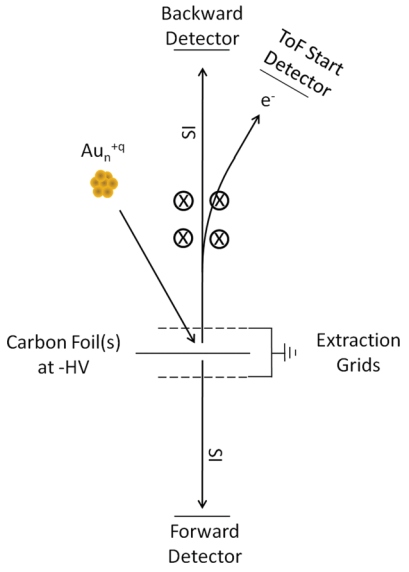

Figure 1. Experimental setup for bidirectional ToF analysis of SIs from thin carbon foils.

Amorphous carbon foils with thicknesses of 5, 15, 20, and 40 nm were obtained from the Arizona Carbon Foil Company (Tucson, AZ). The thickness values given by ACF were monitored by Rutherford Backscattering (and the energy loss by Au_1 at 0° incidence) with the range of the thicknesses being ±15% for a large area. Foils for mass spectrometric analysis were mounted on 81% transmission nickel grids using the foil floating method to transfer the foils from a glass slide to the desired support.[19] The 30° incidence angle of the projectile increases the path length by 15% (5, 15, 20, and 40 nm become 5.8, 17.3, 23.1, and 46.2 nm, respectively).

2.2. SIMS Instrumentation. Gold cluster beams were provided by the 130 kV Pegase platform described in ref 20. The different beams used include Au_3^+ and massive Au_n^{+q} clusters with n/q = 30, 50, 100, and 200. Beam specifications (energy, charge, etc.) are presented in Table 1 with the median charge states extracted from data given in ref 21.

Table 1. Gold Cluster Projectile Characteristics

n/q	$\langle q \rangle$	energy/q (keV)	energy/at (keV/at)	total energy (keV)	$n^{2/3}$ area[a]	$E_T/n^{2/3}$ energy per unit area[a]
30	3	110	3.7	330	20	16.43
50	3	110	2.2	330	28	11.69
100	4	110	1.1	440	54	8.10
200	5	110	0.55	550	100	5.50
100	4	125	1.25	500	54	9.21

[a]The cross-sectional area and energy per unit area are obtained assuming a ballistic model (i.e., projectile range is proportional to the energy per unit area).

The experiments have been performed event by event with a bombardment rate of less than 1000 Hz where the term event refers to the impact of a single projectile and subsequent detection of emitted secondary ions prior to the impact of the next projectile. The impact frequency is achieved through the use of collimators and kHz range pulsation. A more detailed description of the event by event methodology can be found in ref 22. The n/q selection is monitored by the projectile ToF measurement between the pulsing plates and the detection of electrons emitted backward from the target.

2.3. TEM Analysis. Separate samples were prepared for transmission electron microscopy (TEM) analysis by mounting the 5, 15, and 20 nm foils on copper TEM support grids. These samples were impacted with 130 qkeV Au_{100q}^{+q} projectiles at an impact angle of 45°. Bright field TEM images were then obtained using an FEI Tecnai G^2 F20 ST FE-TEM for impacted and nonimpacted samples of each thickness. All analyses were performed with 200 keV electrons incident normal to the foil surface.

3. RESULTS AND DISCUSSION

3.1. TEM Visualization. Transmission electron microscopy was used to investigate the projectile bombardment. The foils were found to be largely intact, uniform, and free from pinholes. The TEM images provided in Figure 2 show holes

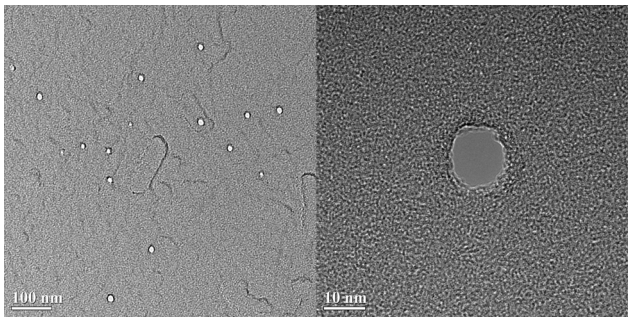

Figure 2. (left) TEM image obtained from a 5 nm thick carbon foil impacted with 130 qkeV Au_{100q}^{+q} projectiles. Projectile tracks appear as lighter circular regions. (right) High magnification image of a hole in the 5 nm foil shows the width of the hole to be approximately 10 nm.

created by 130 qkeV Au_{100q}^{+q} projectiles in a 5 nm carbon foil. For the 5 nm foil, the amorphous carbon is completely removed from the tracks such that a hole is created, as shown by the lack of grainy features inside the hole. Similar holes were also observed for the 15 and 20 nm thick carbon foils, though some amorphous carbon material remains within the tracks either as a result of surface relaxation or incomplete penetration (data not shown). The diameters of holes in the 5 nm foil range from 3 to 12 nm with the majority of holes measuring ~10 nm. Hole diameters in the 15 nm foil are reduced by nearly a factor of 2 relative to holes in the 5 nm foil. Interestingly, the density of holes observed in the 5 and 15 nm foils are similar with ~10^9 holes/cm^2, but the number of holes in the 20 nm foil is drastically reduced. This result suggests that most of the projectiles are unable to pass through the 20 nm foil and therefore brackets their range between 15 and 20 nm. These images provide direct evidence of projectile penetration through the impacted foils and provide a basis for interpreting the results that follow.

3.2. Analysis of Forward and Backward Mass Spectra. The simultaneously acquired forward and backward mass spectra from 125 qkeV Au_{100q}^{+q} projectiles impacting a 15 nm thick carbon foil are presented in Figure 3. The carbon clusters emitted backward (Figure 3a) show an odd−even oscillation similar to that observed with various other energy deposition mechanisms (e.g., collisional and electronic sputtering and laser ablation) on different carbon structures.[23−26] The well-studied backward cluster emission, with maxima of C_n^- occurring for

dx.doi.org/10.1021/jp212126m | J. Phys. Chem. C 2012, 116, 8138−8144

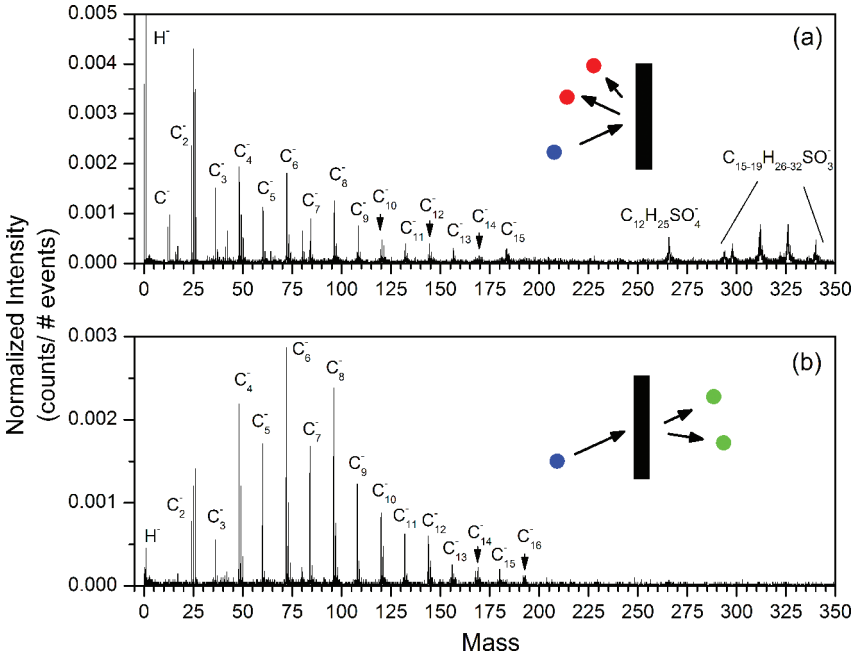

Figure 3. Negative mode ToF mass spectrum obtained in the (a) backward and (b) forward directions from a 15 nm thick carbon foil impacted by 125 qkeV Au_{100q}^{+q} projectiles.

even values of n, is explained by cluster ion fragmentation within the accelerating region.[25] The distribution of coemitted clusters in the forward direction differs significantly from the backward distribution. Another significant difference between the spectra is the near absence of H^- and C^- in the forward mass spectrum. As shown in Figure 3, the emission of molecular ions (lauryl sulfate, $C_{12}H_{25}SO_4^-$, m/z = 265; alkylbenzene sulfonate derivatives, $C_{15-19}H_{26-32}SO_3^-$, m/z = 293, 297, 311, 325, 339, 353) attributed to surfactant chemicals is observed in the backward direction but not in the forward direction. Transfer of the thin carbon foils to experimental mounts entails floating the thin carbon foils on a water surface and then picking them up using the support grid.[19] To determine whether this preparation step causes surfactant elimination from or segregation on one of the foil surfaces, a 15 nm foil was analyzed in both the normal and flipped orientations. Normal orientation is defined as the condition in which the top surface of a floating foil is oriented toward the incoming projectile. Figure 4 shows that surfactant molecular ion emission is observed in the backward direction with only low level surfactant ion emission in the forward direction, regardless of foil orientation. The directional emission of molecular ions is therefore a result of different interaction mechanisms and not an artifact of sample preparation. Unless otherwise stated, all experiments have been performed in the normal orientation. The reproducibility of the results has been measured in the forward direction, with a maximum yield variation of ±12.5%, but no alteration of the carbon cluster distribution. In the backward direction, the ratio $Y(C_n)/Y(C_nH)$ changes by ~20%, with this variation being related to the contribution of the surfactant.

3.3. Experimental parameters. The experimental setup described allows for the study of effects induced by the variation of different instrumental parameters. These parameters and the corresponding observables are summarized in Table 2. For a given energy and cluster size, the range and linear energy loss in a given solid are fixed. Therefore, variation

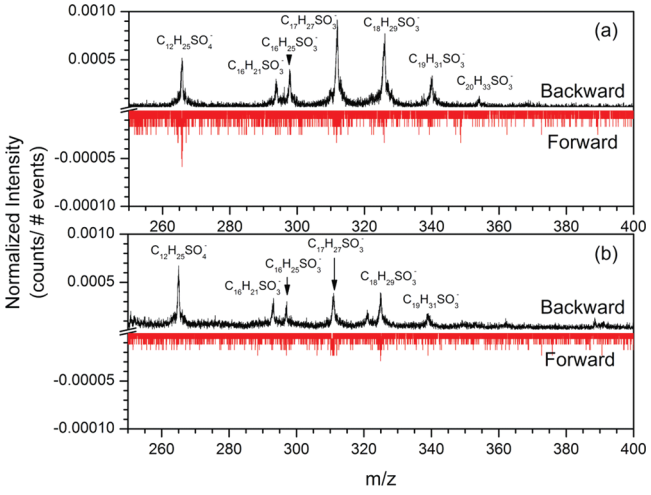

Figure 4. Surfactant molecular ion region of negative mode ToF mass spectra obtained from a 15 nm thick carbon foil impacted by 95 qkeV Au_{100q}^{+q} projectiles in the (a) normal and (b) flipped foil orientations. Forward emission spectra are shown inverted for comparison. Note: forward spectra are magnified 10×.

of the sample thickness permits the observation of the energy density, interaction depth, and energy transfer mechanism in both the forward and backward directions. Similarly, we are able to determine the influence of the energy/velocity for a given projectile and the influence of the projectile size by adjusting these respective variables.

3.4. Effect of Foil Thickness. Figure 5 presents the simultaneously acquired ion yields in the forward and backward directions for three different foil thicknesses. In the case of the 5 nm foil (Figure 5a), the SI yields and the C_n^- cluster distributions are similar for both directions. The momentum transfer process does not play a role in forward emission, and the energy deposited by the projectile in the target volume induces almost the same SI emission. The interaction volume

dx.doi.org/10.1021/jp212126m | J. Phys. Chem. C 2012, 116, 8138–8144

Table 2. Summary of the Information Provided by Various Experimental Parameters

parameters		measurements	information	
beam (Au_n^{+q})	sample	SI emission	backward emission	forward emission
velocity and n fixed	thickness	yields as f(thickness)	depth of interaction	depth of interaction or attenuation range
velocity and n fixed	thickness	cluster distribution as f(thickness)	depth of interaction, electronic excitation, coherent effect	coherent motion signature
velocity for a fixed n	thickness	yields as f(thickness), cluster distribution as f(thickness)	influence of the impact energy	range as f(V), energy loss as f(V), coherent motion
n for a given velocity	thickness	yields as f(thickness), cluster distribution as f(thickness)	influence of n	range as f(n), coherent motion, energy loss as f(n)

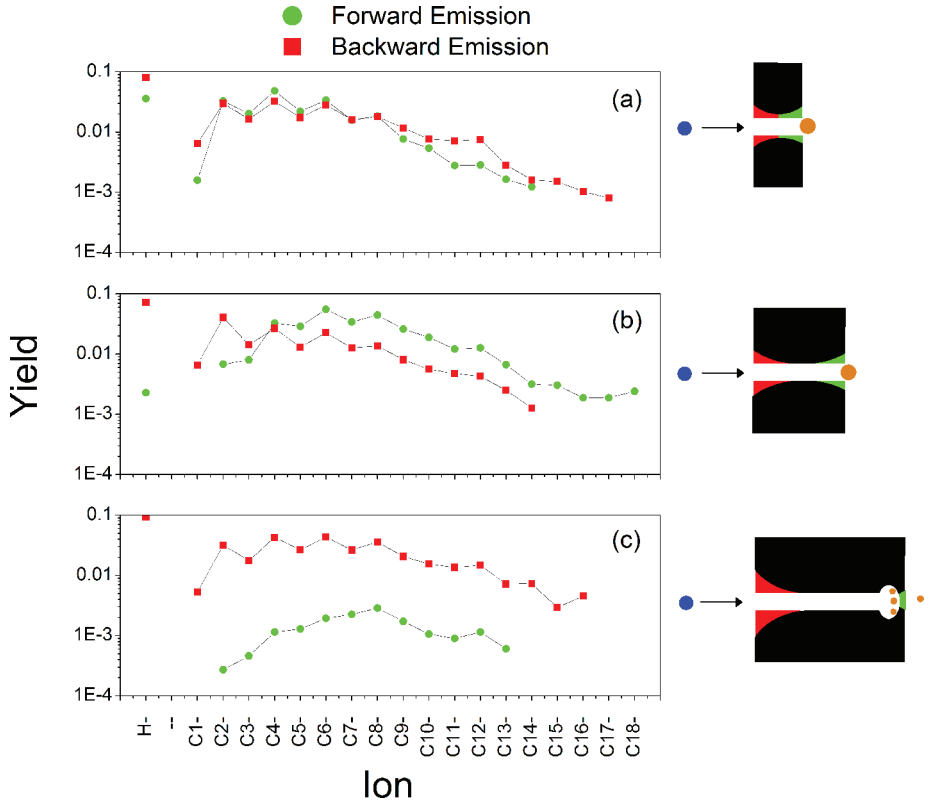

Figure 5. Yields for H^- and carbon cluster (C_n^-) species obtained in the forward and backward directions from (a) 5, (b) 15, and (c) 20 nm thick carbon foils impacted by 125 qkeV Au_{100q}^{+q} projectiles; corresponding interaction figures shown on right.

and ion formation process are the same for both sides of the foil. This is supported by the observation of H^-, C^-, and C_2^- and similar C_nH^- distributions (data not shown). For the 15 nm foil (Figure 5b), C_n^- and C_nH^- distributions are different between the two directions. The backward emission is similar to that obtained with the 5 nm carbon foil with H^-, C^-, and C_2^- emission and a C_n^- distribution slightly shifted to larger clusters. This comparison indicates that the emission process does not change drastically and that the energy available for emission increases for the thicker foil. Concerning the forward emission, there is a significant shift toward carbon clusters with a high number of constituents as shown in Figure 5. There is an increase of the total ion emission but a decrease in the yields of light ions such as H^-, C^-, CH^-, and C_2^-. These results indicate that the emission process is different for the two sides and that the energy deposited in the solid is probably higher than that in the 5 nm case. These two points are attributed to the increased interaction volume, where more projectile energy can be deposited. In the case of the 20 nm foil (Figure 5c), the forward and backward carbon cluster distributions are similar to the previous 15 nm foil. The yields do not change for the backward direction, though a small shift toward higher mass is observed in the carbon cluster distribution relative to the 15 nm foil. These results indicate that the forward and backward emission processes do not change for the 15 and 20 nm foils. The backward SI yields are almost equal to the previous values, a sign that the plateau for energy deposition has been reached. In other words, the increased foil thickness does not increase the amount of energy useful for backward SI emission. Therefore, the depth of interaction must be smaller than 17.3 nm (15 nm/sin 30°). On the contrary, the increase of the thickness from 15 to 20 nm induces a decrease of the forward SI emission by a factor of 10 without modification of the carbon cluster distribution. The rate of H^-, C^-, CH^-, and C_2^- emission disappears or is very low. The two consequences of this observation are that the added distance of 5.8 nm introduces an important attenuation for the energy transfer to the surface and that the depth of interaction for forward emission is less than 5.8 nm. The slowing down of the projectile leads to a decrease of the energy deposited at the foil surface facing the forward

dx.doi.org/10.1021/jp212126m | J. Phys. Chem. C 2012, 116, 8138–8144

direction. This result allows the range of the Au_{100q}^{+q} massive projectile in amorphous carbon at these energies to be bracketed between 15 and 20 nm, which is consistent with the TEM results. This range value is less than that predicted by a ballistic description of the hypervelocity penetration,[27] where the theoretical range is proportional to the kinetic energy per cross-sectional area, as given in Table 1. Such a deviation can be explained by a significant plastic deformation and fragmentation of the projectile on impact which increases the effective cross-sectional area and causes additional slowing. The measured range lies between that of equal velocity atomic ions (3−6 nm for this energy range) and the range calculated from a ballistic model (~100 nm).

The carbon cluster yields can be approximated by log-normal distributions as seen in Figure 6. These curves show the

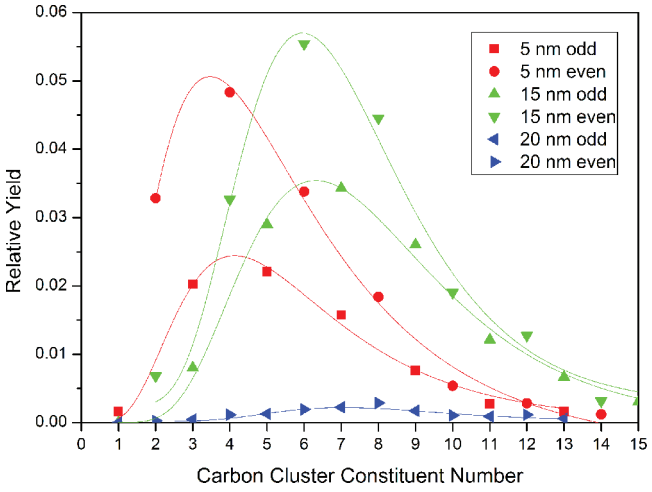

Figure 6. Log-normal fits of the odd and even carbon cluster distributions of 5, 15, and 20 nm carbon foils observed in the forward direction.

increase of the average mass of the C_n^- distribution as a function of the thickness for forward emission. The odd and even carbon clusters are addressed independently to show that the log-normal fits have nearly the same function for each, despite the oscillatory nature of the yields. The curves show a general shift toward larger average cluster size with the increasing foil thickness, despite the yield reduction for the 20 nm foil. Analysis of the backward spectra (data not shown) reveals two contributions to the final cluster distribution: one for the light carbon species (C^-, C_2^-, and C_3^-) and a second for the larger clusters. It appears that the mechanism for creation of lighter species is absent in the case of forward emission.

3.5. Effect of Projectile Size and Energy. Forward and backward SI emission from a 15 nm thick carbon foil impacted by the gold trimer and various massive gold clusters are shown in Figure 7. The interaction of Au_3^+ with a solid is very well-defined, in particular for forward emission where only the independent collision cascades play a role. In this case, only atomic ions and small carbon clusters are emitted. The backward spectrum reveals the emission of larger carbon clusters out to C_{14}^- but with yields 2−3 orders of magnitude lower than the massive projectiles. Concerning the massive clusters, the backward SI yields and carbon cluster distributions are the same for all massive cluster projectiles. The process of emission does not change with the nanodroplet constituent

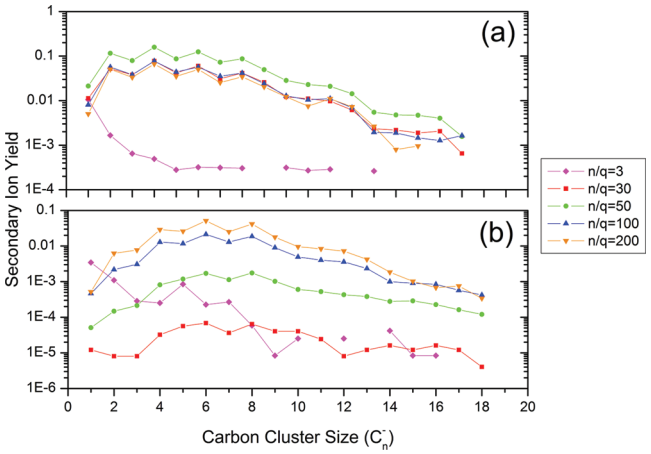

Figure 7. Negative ion yields for H^- and carbon cluster species obtained in the (a) backward and (b) forward directions from a 15 nm thick carbon foil impacted by various size Au_n^{+q} clusters at 110 qkeV.

number from 90 to 1000 gold atoms. The nearly constant value of the SI yields, regardless of the projectile, is surprising because with this set of projectiles, the nanodroplet cross-section increases by a factor of 5, the total energy by a factor of 2, and the range in the frame of a ballistic approach decreases by a factor of almost 3. The forward SI yields present a two order increase as a function of the projectile constituent number (n). This pronounced behavior does not largely affect the carbon cluster distribution. The process of ionic emission does not change, but the results indicate that the slowing down of the smaller particles is much quicker than that of the heavier particles, in spite of a much higher initial velocity. This observation contradicts the ballistic approach, which may not apply in this velocity range. Also, for these clusters that have a majority of atoms at the surface of the projectile, atoms can be easily stripped or peeled during the penetration such that the shrinking or fragmentation of the projectile ultimately leads to the shorter range. For heavy particles, this process exists, but the inner core constitutes a more significant portion of the projectile, and stripping does not significantly reduce the size of the projectile.

The main result from this experiment is that the forward carbon cluster distribution is not affected by the massive projectile size or velocity; only the yields are increased for larger or faster projectiles. The forward emitted H^-, C^-, and C_2^- yields increase more rapidly than the larger carbon clusters. The ionic emission of light elements requires processes that can only occur when the projectile velocity is not too low at the exit surface. Projectile passage across the surface leads to electronic excitation, allowing for an electron attachment mechanism. The larger carbon clusters are likely due to an adiabatic expansion.[28] In the forward direction, the preponderance of C_4^-, C_6^-, and C_8^- vs C_2^- is attributed to a large pressure drop when compressed matter reaches the foil exit. The preponderance of C_2^- vs C_4^-, C_6^-, and C_8^- in the backward direction suggests a lower pressure drop at the foil entrance. We should also note enhanced probability of electron attachment for the large lower velocity clusters.[29]

In Figure 8, backward and forward SI yields for the $n/q = 100$ projectile at 95, 110, and 125 qkeV are given. Within this energy range, there is only a moderate increase in SI yields. This result is interpreted as a threshold for projectile energy, such that at these energies, the projectile is able to fully

dx.doi.org/10.1021/jp212126m | J. Phys. Chem. C 2012, 116, 8138−8144

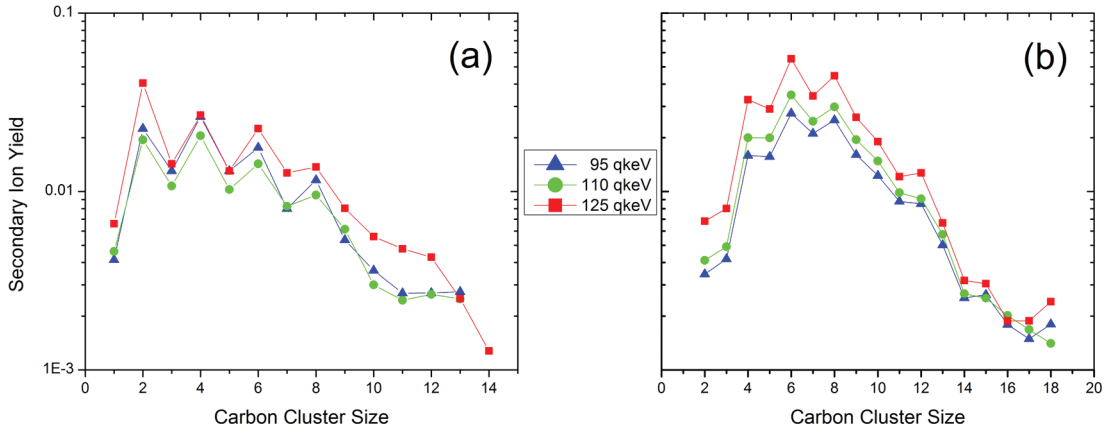

Figure 8. Carbon cluster ion yields in the (a) backward and (b) forward directions from a 15 nm thick carbon foil as a function of projectile energy.

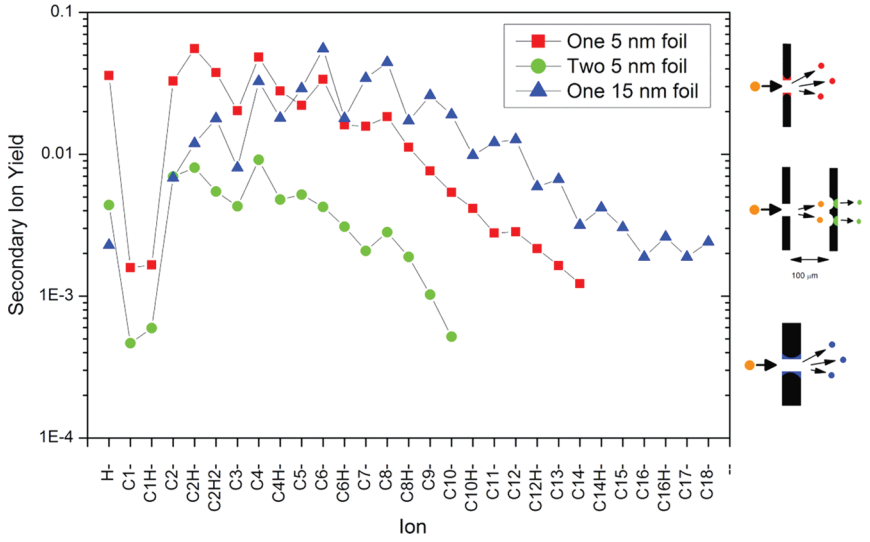

Figure 9. Forward SI yields from a single 5 nm, two stacked 5 nm, and a single 15 nm carbon foil impacted by 125 qkeV Au_{100q}^{+q}; corresponding interaction figures shown on right.

penetrate the foil, and much of the excess kinetic energy is retained by the projectile atoms rather than imparted to the foil. Figure 7 more clearly reveals this plateau of SI emission for the 15 nm thick carbon foil as a result of the massive cluster size. There is a clear threshold of projectile size that develops, such that the n/q = 30 and n/q = 50 projectiles are not capable of generating the maximum SI yields due to their supposed range limitations. This suggests that the n/q = 100 and n/q = 200 projectiles at these energies are able to fully penetrate the 15 nm foil and deposit similar amounts of energy at the exit surface.

3.6. Fate of the Massive Projectile. As mentioned above, determining the fate of the projectile is critical for understanding the interaction it has within the solid. It is possible to observe the final state of the projectile after passage through the foil indirectly by monitoring the forward SI emission. Figure 9 shows the forward SI yields from a single 5 nm foil as compared to two 5 nm foils separated by a 100 μm wide gap between. We observe an order of magnitude reduction in the SI yields between the single and double foil targets while maintaining nearly identical cluster distributions. It may be noted that the total thickness of the stacked foils is less than the 15 nm foil, which gives abundant forward emission. Using SI emission as an indicator for projectile transmission, we can assume that less than 10% of the projectiles penetrate the second foil sufficiently to cause emission in the forward direction. The most likely cause for this reduction is that the projectile fragments significantly at the exit of the first foil, generating smaller projectiles at low velocities, which go on to impact the second foil. If the projectile retained most of its mass, then we would expect total ion yields comparable with the 5 and 15 nm thick carbon foils, signaling complete penetration. Instead, the data suggests that during passage within the solid, the massive gold cluster exhibits a cohesive motion between its constituents, which is capable of generating energy deposition conditions suitable for large carbon cluster emission. In other words, the atoms of the cluster travel through the material in close proximity to one another, even up to depths of 20 nm. However, in the case when the cluster reaches the exit of the solid, the high charge state and internal energy of the projectile likely results in fragmentation/Coulomb explosion, which reduces the projectile to atomic and small polyatomic components. This assumption of a high charge state has been used previously to explain the high emission yields of H^+, H_2^+, H_3^+, and C^+ observed in the backward direction.[30] There are some clusters within the size distribution of the beam that may retain a central core after penetration through the first foil,

dx.doi.org/10.1021/jp212126m | J. Phys. Chem. C 2012, 116, 8138–8144

which can continue on to cause forward emission from the second foil.

4. CONCLUSIONS

We show that the foil thickness determines the observable cluster distribution for forward emitted ions, with thicker foils giving distributions shifted toward larger clusters. This observation reveals a new mechanism for ion emission based on the massive gold clusters' ability to physically push material out of the carbon foil. The process can be considered mesoscopic in nature, akin to hydrodynamic penetration. The momentum of the projectile is more efficiently transferred to the ejecta as translational energy as opposed to internal, vibrational excitation. The reduction in energy density at the exit surface can also be deduced from the virtual absence of light ions in the mass spectrum. We suggest that carbon clusters emitted in the forward direction have a lower average internal energy than the corresponding backward-emitted clusters. This work also gives tangible evidence of projectile size dependent ranges proposed by previous theoretical work as a clearing-the-way effect. The ranges are larger than atomic ions of the same velocity (between 3 and 6 nm in our experiments) but are five to ten times lower than values predicted by a ballistic model. Using a dual foil experiment, we are able to indirectly observe the disintegration of the massive gold clusters at the exit of a thin foil. During passage through a solid, the gold cluster constituent atoms are minimally scattered, i.e., they travel in a coherent motion. For foil thicknesses that are less than the projectile range, the impact energy cannot be dissipated, and the projectile will fragment once it is no longer confined within the solid.

AUTHOR INFORMATION

Corresponding Author

*Tel: 979-845-2341. Fax: 979-845-1655. E-mail: schweikert@chem.tamu.edu.

Notes

The authors declare no competing financial interest.

ACKNOWLEDGMENTS

This work was supported by the National Science Foundation (Grant CHE-0750377). F.A.F.-L. acknowledges the National Institute of Health support (Grant No. 1K99RR030188-01). J.D.D. acknowledges a fellowship from the U.S. Department of Homeland Security. Transmission electron microscopy imaging was performed by Hansoo Kim at the Texas A&M Microscopy & Imaging Center.

REFERENCES

(1) Eller, M. J.; Verkhoturov, S. V.; Della-Negra, S.; Schweikert, E. A. *J. Phys. Chem. C* **2010**, *114*, 17191−17196.
(2) Brenes, D. A.; Garrison, B. J.; Winograd, N.; Postawa, Z.; Wucher, A.; Blenkinsopp, P. *J. Phys. Chem. Lett.* **2011**, *2*, 2009−2014.
(3) Le Beyec, Y. *Int. J. Mass Spectrom. Ion Processes* **1998**, *174*, 101−117.
(4) Jacquet, D.; Le Beyec, Y. *Nucl. Instrum. Methods Phys. Res., Sect. B* **2002**, *193*, 227−239.
(5) Verkhoturov, S. V.; Eller, M. J.; Rickman, R. D.; Della-Negra, S.; Schweikert, E. A. *J. Phys. Chem. C* **2009**, *114*, 5637−5644.
(6) Beuhler, R. J.; Friedman, L. *J. Phys. Colloq.* **1989**, C2.
(7) Baudin, K.; Brunelle, A.; Della-Negra, S.; Jacquet, D.; Håkansson, P.; Le Beyec, Y.; Pautrat, M.; Pinho, R. R.; Schoppmann, C. *Nucl. Instrum. Methods Phys. Res., Sect. B* **1996**, *112*, 59−63.
(8) Beuhler, R.; Friedman, L. *Chem. Rev.* **1986**, *86*, 521−537.
(9) Guillermier, C.; Della-Negra, S.; Schweikert, E. A.; Dunlop, A.; Rizza, G. *Int. J. Mass Spectrom.* **2008**, *275*, 86−90.
(10) Dunlop, A.; Jaskierowicz, G.; Ossi, P. M.; Della-Negra, S. *Phys. Rev. B: Condens. Matter* **2007**, *76*, 155403.
(11) Anders, C.; Urbassek, H. M. *Nucl. Instrum. Methods Phys. Res., Sect. B* **2007**, *258*, 497−500.
(12) Anders, C.; Urbassek, H. M. *Nucl. Instrum. Methods Phys. Res., Sect. B* **2005**, *228*, 57−63.
(13) Andersen, H. H.; Johansen, A.; Olsen, M.; Touboltsev, V. *Nucl. Instrum. Methods Phys. Res., Sect. B* **2003**, *212*, 56−62.
(14) Shulga, V. I.; Sigmund, P. *Nucl. Instrum. Methods Phys. Res., Sect. B* **1990**, *47*, 236−242.
(15) Bouneau, S.; Brunelle, A.; Della-Negra, S.; Depauw, J.; Jacquet, D.; Le Beyec, Y.; Novikov, A.; Pautrat, M.; Andersen, H. H. *Nucl. Instrum. Methods Phys. Res., Sect. B* **2006**, *251*, 383−389.
(16) Delcorte, A.; Garrison, B. J.; Hamraoui, K. *Anal. Chem.* **2009**, *81*, 6676−6686.
(17) Srama, R.; Woiwode, W.; Postberg, F.; Armes, S. P.; Fujii, S.; Dupin, D.; Ormond-Prout, J.; Sternovsky, Z.; Kempf, S.; Moragas-Klostermeyer, G.; Mocker, A.; Grün, E. *Rapid Commun. Mass Spectrom.* **2009**, *23*, 3895−3906.
(18) Ledbetter, M. C.; Beuhler, R. J.; Friedman, L. *Proc. Natl. Acad. Sci. U.S.A.* **1987**, *84*, 85−88.
(19) The Arizona Carbon Foil Company. *ACF-Metals Product Information Manual*, 2010; pp 1−26.
(20) Della-Negra, S.; Arianer, J.; Depauw, J.; Verkhoturov, S. V.; Schweikert, E. A. *Surf. Interface Anal.* **2011**, *43*, 66−69.
(21) Bouneau, S.; Della-Negra, S.; Depauw, J.; Jacquet, D.; Le Beyec, Y.; Mouffron, J. P.; Novikov, A.; Pautrat, M. *Nucl. Instrum. Methods Phys. Res., Sect. B* **2004**, *225*, 579−589.
(22) Rickman, R. D.; Verkhoturov, S. V.; Hager, G. J.; Schweikert, E. A.; Bennett, J. A. *Int. J. Mass Spectrom.* **2005**, *241*, 57−61.
(23) Feld, H.; Zurmuehlen, R.; Leute, A.; Benninghoven, A. *J. Phys. Chem.* **1990**, *94*, 4595−4599.
(24) Diehnelt, C. W.; Van Stipdonk, M. J.; Schweikert, E. A. *Phys. Rev. A: At. Mol. Opt. Phys.* **1999**, *59*, 4470−4474.
(25) Gnaser, H. *Nucl. Instrum. Methods Phys. Res., Sect. B* **1999**, *149*, 38−52.
(26) Fernandéz-Lima, F. A.; Ponciano, C. R.; da Silveira, E. F.; Nascimento, M. A. C. *Chem. Phys. Lett.* **2007**, *445*, 147−151.
(27) Herrmann, W.; Wilbeck, J. S. *Int. J. Impact Eng.* **1987**, *5*, 307−322.
(28) Hilf, E. R.; Tuszynski, W.; Curdes, B.; Curdes, J.; Wagner, M.; Wien, K. *Int. J. Mass Spectrom. Ion Processes* **1993**, *126*, 101−114.
(29) Gnaser, H. *Phys. Rev. B: Condens. Matter* **2001**, *63*, 045415.
(30) Della-Negra, S.; Depauw, J.; Guillermier, C.; Schweikert, E. A. *Surf. Interface Anal.* **2011**, *43*, 62−65.